Low-energy electron scattering from cyanamide

Kedong Wang,* Shuangcheng Guo, Ju Meng, and Xiaotian Huang
College of Physics and Materials Science, Henan Normal University, Xinxiang 453007, People's Republic of China

Yongfeng Wang
Key Laboratory of Neutronics and Radiation Safety, Institute of Nuclear Energy Safety Technology, Chinese Academy of Sciences, Hefei 230031, People's Republic of China

(Received 19 May 2016; published 7 September 2016)

The low-energy electron collisions with cyanamide molecule are investigated by using the UK molecular R-matrix codes for electron energies ranging from 0.01 eV to 10 eV. Three models including static-exchange, static-exchange plus polarization, and close-coupling (CC) approximations are employed to reveal the dynamic interaction. Elastic (integrated and differential), momentum-transfer, and excitation cross sections from the ground state to the three low-lying electron excited states have been presented. Two shape resonances, two core-excited resonances, and two Feshbach resonances are detected in the CC approximation. The role of active space in the target and scattering problem including the resonances is discussed. The precise resonance parameters are found to be sensitive to the treatment of polarization effects employed. These resonances may be responsible for the fragments observed in a recent experiment of the dissociative electron attachments to cyanamide. Since the cyanamide molecule has a large permanent dipole moment, a Born closure procedure is used to account for the contribution of partial waves higher than $l = 4$ to obtain converged cross sections.

DOI: 10.1103/PhysRevA.94.032703

I. INTRODUCTION

Electron-molecule collisions are of fundamental importance for astrophysics, atmospheric physics, and bio-physics, and have many applications in plasmas physics and fusion science [1]. The recent discovery that low-energy electrons can induce strand breaks in DNA has renewed interest in electron collisions with biomolecules [2]. Despite a growing demand for electron-assisted data (cross sections, transport coefficients), due to difficulty in accurate representation of the target wave function and polarization between scattering electron and target, the accurate simulation of electron-molecule scattering at low energies still remains a computational challenge.

Cyanamide, NH_2CN, is an important astrophysical molecule observed in the gas clouds of the interstellar medium (ISM) and can be synthesized by heterogeneous chemistry on interstellar dust grains [3]. It was a natural product formed in some kinds of plants [4]. It was also suggested that cyanamide was present on the primitive earth where its production was possible by electron irradiation of methane, ammonia, and water mixture or by the ultraviolet irradiation of aqueous NH_4CN. Furthermore, cyanamide is recognized as a fundamental probiotic and an important precursor molecule in the study of the origin of life [5]. In addition, as one of the simplest organic molecules comprising important organic groups (cyano and amide), cyanamide could serve as a model molecule for more complex species with biological relevance. Because of these reasons, it is interesting to study low-energy electron scattering with cyanamide.

Until now interactions of electron with cyanamide molecule have not been investigated thoroughly, due to both experimental and theoretical challenges. To our knowledge, the only available measurement was reported for dissociative electron attachment to cyanamide by Tanzer *et al.* [6], who used crossed electron-molecular beams. They detected the following anionic species: $NHCN^-$, NCN^-, CN^-, NH_2^-, NH^-, and CH_2^-. The anions are formed at two broad major resonance regions, one between about 0.5 and 4.5 eV and the other between 4.5 and 12 eV. Combining with the calculated thermochemical data, the possible reaction channels for all measured negative ions were discussed.

In this paper we performed *ab initio* calculations of integral elastic and electronically inelastic cross sections for low-energy electrons scattering from cyanamide within the fixed-nuclei (FN) approximation. For this purpose, we have used the UK R-matrix polyatomic code [7]. The R-matrix method can describe correlation effects well and gives an adequate representation of target molecules and the continuum electrons. This method has proved to be reliable in a series of studies on the polyatomic molecules [8–10]. Our interest lies in low-energy region ($\leqslant$10 eV), where high-level but few-channel methods such as the R matrix work well. It provides cross sections at a large number of scattering energies efficiently. The incoming electron can occupy one of the many unoccupied molecular orbitals, or can excite any of the occupied molecular orbitals (MOs) as it falls into another one, which is known as a resonance. Cross sections for all these processes can show features, usually enhancements, due to resonances. In the present work, we investigate these processes within static-exchange (SE), static-exchange plus polarization (SEP), and close-coupling (CC) approximations for the electron-scattering calculations for cyanamide.

II. COMPUTATIONAL DETAILS

A. Theoretical method

The R-matrix theory was described in detail elsewhere [11,12]; we only give an outline here. In a fixed nuclei R-matrix

*wangkd@htu.cn

approach, the configuration space is divided into an inner region and an outer region. The inner region is defined as the volume of a sphere centered at the center-of-mass of the target molecule. In the inner region, the scattering electron is indistinguishable from the electrons of the target. The electron-electron correlation and exchange are strong. The short-range correlation effect is essential for accurate prediction of differential cross section (DCS) at large scattering angle and the exchange effect is important for the spin-forbidden excitation cross section. In the outer region, it is assumed that the scattering electron can be considered to be distinct. This electron therefore moves in a local potential arising from its long-range interaction with the target. The electron exchange and correlation effects between the scattering electron and target electrons are neglected.

In the inner region, the wave function of the $(N+1)$-electron system is expanded in terms of

$$\Psi_k(x_1,\ldots,x_{N+1}) = \mathcal{A}\sum_{ij}\bar{\Phi}_i(x_1,\ldots,x_N;\hat{\mathbf{r}}_{N+1}\sigma_{N+1})\,r_{N+1}^{-1}B_j \times(r_{N+1})\,a_{ijk} + \sum_i \chi_i(x_1,\ldots,x_{N+1})\,b_{ik}. \tag{1}$$

Here the $\bar{\Phi}_i$ denote the channel functions constructed from the N-electron target states, and $\mathcal{A}$ is an antisymmetrization operator, while x_N is the spatial and spin coordinate of the Nth electron, represents the ith state of the N-electron target, $B_j(r)$ represent the continuum orbitals. The χ_i are additional $(N+1)$-electron bound states. Coefficients a_{ijk} and b_{ik} are variational parameters determined as a result of the matrix diagonalization. The sum in the second term of Eq. (1) represents the short-range correlation and polarization effects, running over all configurations for $(N+1)$ electrons that are L^2 functions. These are also important for relaxing the orthogonality imposed between the target and continuum orbitals.

In the outer region, exchange between the scattering electron and electrons of the target is neglected and a single center expansion of the electron-molecule interaction is used. The R matrix is constructed and propagated to a radius large enough so that an asymptotic expansion for the radial wave functions of the scattering electron in each channel can be used.

DCSs were calculated following the procedure implemented in the program POLYDCS [13]. The general theory of the scattering of an electron from a polyatomic molecule in the FN approximation has been presented many times before, for example, the review by Gianturco and Jain [14]. The DCS is thus given by the expression

$$\frac{d\sigma}{d\Omega} = \frac{d\sigma^B}{d\Omega} + \sum_L (A_L - A_L{}^B)P_L(\cos\theta), \tag{2}$$

where $P_L(\cos\theta)$ is the Legendre function and A_L are coefficients which depend explicitly on products of T-matrix elements and on algebraic factors. The superscript B denotes that the relevant quantity is calculated within the dipolar Born approximation. The quantity $\frac{d\sigma}{d\Omega}$ for any initial rotor state $|J\tau\rangle$ is given by the sum over all the final rotor states $|J'\tau'\rangle$:

$$\frac{d\sigma^B}{d\Omega} = \sum_{J'\tau'}\frac{d\sigma^B}{d\Omega}(J\tau \to J'\tau'). \tag{3}$$

The expression for the state-to-state rotationally inelastic DCS, $\frac{d\sigma^B}{d\Omega}(J\tau \to J'\tau')$ for a spherical top, a symmetric top, and an asymmetric top molecule has been discussed by Sanna and Gianturco [13]. The MTCS is calculated similarly by

$$\sigma_m = 2\pi\int\frac{d\sigma}{d\Omega}(1-\cos\theta)d\theta. \tag{4}$$

B. Target models

Cyanamide is a close-shell molecule which has $X\,^1A'$ ground state in the C_s point group. The structural parameters optimized at B3LYP/6-31+G** level (three bonds of N-C = 1.167 Å, C-N = 1.344 Å, and N-H = 1.012 Å, three angles of N-C-N = 177.242°, C-N-H = 115.934°, and H-N-H = 114.048°) are used in the present calculations. The Hatree-Fock (HF) self-consistent field (SCF) calculations with three different basis sets (6-31G*, cc-pVDZ, and cc-pVTZ) are tested to obtain the reliable wave function. We did not use the diffuse functions, as they would extend outside the R-matrix box. These calculations at different levels give the same electronic configuration at the ground state ($1a'^2 \sim 9a'^2$; $1a''^2 \sim 2a''^2$). The complete active space (CAS) configuration interaction (CI) method was used to represent the target states. In the CI model, all possible configurations (only restricted by the space-spin symmetry of the problem) resulting from the distribution of a set of active electrons among a set of valence molecule orbitals are taken into account. Therefore, the target electronic states are represented at a partially correlated level. In the present work, twelve frozen electrons were distributed in the $1a'^2 \sim 6a'^2$ configuration, and the remaining ten electrons are allowed to move freely in the active space (11, 4) including MOs $7a'^2 \sim 11a'^2$ and $1a''^2 \sim 4a''^2$. The naming method for the active space will be used throughout in the present paper.

Table I lists vertical excited energies and dipole moments of neutral cyanamide in our CI model with different basis

TABLE I. Vertical excited energies (in eV) and the ground-state dipole moment (in D) as a function of basis sets. The (11, 4) active space is used.

State	6–31 G	cc-pVDZ	cc-pVTZ
$X\,^1A'$	0	0	0
$1\,^3A'$	6.89	6.98	7.16
$1\,^3A''$	7.00	7.05	6.63
$2\,^3A'$	7.75	7.52	7.42
$1\,^1A''$	7.57	7.62	7.57
$2\,^1A'$	8.41	7.91	7.68
$3\,^3A'$	8.03	7.93	8.00
$3\,^1A'$	9.03	9.05	8.96
$2\,^3A''$	8.96	9.07	9.28
$3\,^3A''$	9.27	9.33	9.31
$2\,^1A''$	9.94	9.95	9.68
$3\,^1A''$	10.43	10.17	9.81
$\mu(X\,^1A')$	4.49	4.45	4.60

TABLE II. Vertical excited energies (in eV) and the ground-state dipole moment (in D) as a function of basis sets and active spaces in a 12-state CI model.

	(10,5)		(11,4)		(12,4)		(11,6)	
State	6–31 G	cc-pVDZ	6–31 G	cc-pVDZ	6–31 G	cc-pVDZ	6–31 G	cc-pVDZ
$X\,^1A'$	0	0	0	0	0	0	0	0
$1\,^3A'$	6.60	6.63	6.89	6.98	7.23	6.97	6.65	6.81
$1\,^3A''$	6.50	6.58	7.00	7.05	7.51	7.04	7.19	7.30
$2\,^3A'$	7.82	7.63	7.75	7.52	7.71	7.38	7.92	8.02
$1\,^1A''$	7.05	7.10	7.57	7.62	8.00	7.60	7.90	7.92
$2\,^1A'$	8.39	8.05	8.41	7.91	8.25	7.78	9.11	8.68
$3\,^3A'$	12.24	11.62	8.03	7.93	8.24	7.92	8.78	8.48
$3\,^1A'$	12.26	11.81	9.03	9.05	9.19	9.04	9.38	9.34
$2\,^3A''$	8.59	9.01	8.96	9.07	9.04	9.07	8.58	9.31
$3\,^3A''$	10.12	9.88	9.27	9.33	9.63	9.29	9.28	9.42
$2\,^1A''$	10.07	10.14	9.94	9.95	9.76	9.85	10.01	9.95
$3\,^1A''$	10.54	10.46	10.43	10.17	10.59	10.08	10.09	10.38
$\mu(X\,^1A')$	4.53	4.45	4.50	4.45	4.47	4.42	4.54	4.47

sets in the active space (11, 4). A very good reproduction of the target properties assures a very good target model, which in turn guarantees reliable collision cross-section data. The ground-state dipole moment calculated with cc-pVDZ basis set is 4.45 D, which is closest to the experimental value 4.32 D compiled by NIST [15]. Therefore, the cc-pVDZ basis set is chosen for the final scattering calculations. Based on this model, the rotational constants of cyanamide are determined to be $A = 10.1693\ \mathrm{cm}^{-1}$, $B = 0.3302\ \mathrm{cm}^{-1}$, and $C = 0.3221\ \mathrm{cm}^{-1}$, which are in good agreement with the experimental values ($A = 10.4112\ \mathrm{cm}^{-1}$, $B = 0.3379\ \mathrm{cm}^{-1}$, and $C = 0.3291\ \mathrm{cm}^{-1}$) measured by the Fourier transform infrared rotation-vibration spectrum [16].

It is well known that a larger active space would give rise to additional correlation effects and increase correlation energy, and hence produce better results. But in fact one has to make a compromise due to the limited computer resource. In the present paper, according to our computational capacity, we test several different active spaces: ten electrons distributed in (10, 5), (11, 4), and (12, 4), and eight electrons distributed in (11, 6). The obtained vertical excitation energies, and ground-state dipole moment for these different active spaces are listed in Table II. It is reasonable that different active spaces predict different vertical excitation energies. The dipole moment based on cc-pVDZ basis set is smaller the 6–31 G result, and is closer to the measured value. Then we used cc-pVDZ basis set for the latter scattering calculations in different active space to check the correlation effects. There is no experimental value of the vertical excitation energies available in the literature to compare with the present work.

C. Scattering model

Three different scattering models are used in the present calculations. The first model is the SE model in which the target wave function is not allowed to relax, or polarize, in response to the incoming electron. The SE approximation does give shape resonances, although these are usually too high in energy since their position is lowered by the inclusion of attractive target polarization effects. The second model used is the SE plus polarization (SEP) model in which single excitations out of the HF wave function are used to represent target polarization effects. The SEP model can give good resonance parameters for shape resonances and is also capable of representing Feshbach resonances although this is often more problematic. The final model is the CC model in which 12 target states are introduced into the first sum in Eq. (1). These target states are usually performed by the CI model. CC calculations are particularly good at representing Feshbach resonances associated with the target excited states explicitly included in the CC expansion. However, CC calculations tend to be considerably more computationally expensive than SE or SEP calculations. The 12-state CI calculations were carried out using different active spaces, as mentioned above. The large number of CSF in target calculations in the active space (12, 4) including ten active electrons made scattering calculations intractable. Then the present scattering calculations are confined to ten active electrons in active spaces (10, 5) and (11, 4), and eight electrons in (11, 6).

Our scattering calculations are performed for doublet spin scattering states with A' and A'' symmetries. The continuum orbitals up to g-partial waves ($l \leqslant 4$) are orthogonalized to the target orbitals based on the mixture of Schmidt and Löwdin symmetric orthogonalization and represented by GTOs centered at the molecular center of gravity [17]. The continuum orbitals with an overlap of less than 2×10^{-17} are removed [18]. The radius of the R-matrix box is $12a_0$. Compared with larger radius of the R-matrix box $15a_0$, no distinct changes about the calculation results are founded.

III. RESULTS

A. Static-exchange and static-exchange-polarization scattering calculations

In Fig. 1 we plot the present elastic cross section of cyanamide based on SE and SEP models. The SE model predicts two broad peaks in the total cross section at 5.06 eV and 6.51 eV, respectively. From the two component cross sections, we find that the resonance at 5.06 eV comes

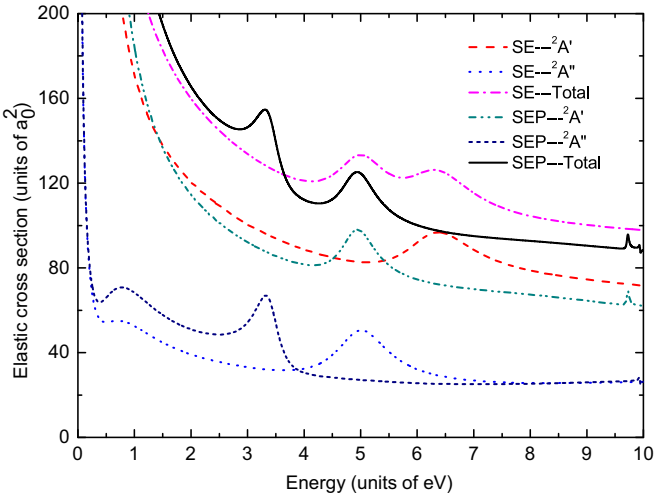

FIG. 1. Elastic cross sections of the electron collision with cyanamide in the static-exchange (SE) and static-exchange-polarization calculations (SEP).

TABLE III. Parameters of identified *e*-cyanamide resonances (in eV). (AS means active space.)

State	Type	Parent state	AS	Position	Width
$^2A''$	*Shape*	$X\,^1A'$	(11,4)	4.25	0.80
			(10,6)	4.01	0.67
			(11,6)	4.25	0.80
$^2A'$	*Shape*	$X\,^1A'$	(11,4)	6.04	1.33
			(11,6)	5.90	1.33
$^2A'$	*Feshbach*	$2\,^3A'$	(11,4)	7.22	0.02
			(10,6)	7.20	0.02
			(11,6)	8.24	0.08
$^2A''$	*Feshbach*	$1\,^1A''$	(11,4)	7.59	0.02
			(10,6)	8.21	0.01
			(11,6)	7.90	0.03
$^2A'$	*Core-excited*	$2\,^3A'$	(11,4)	7.93	0.21
			(11,6)	8.88	0.02
$^2A'$	*Core-excited*	$3\,^1A'$	(11,4)	9.06	0.08
			(11,6)	9.35	0.07

from $^2A''$ symmetry with a width of 1.33 eV. This resonance is called π^* resonance since the incident electron is captured in a virtual π^* MO of cyanamide. When the incident electron occupies a virtual σ^* MO of cyanamide, a σ^* resonance is formed. The other resonance at 6.51 eV is from the $^2A'$ symmetry with a width of 2.00 eV, and belongs to the σ^* resonance. The SE model gives shape resonances that are usually too high in energy for not taking polarization effects into account. To improve the resonance parameters, SEP calculations including the polarization effects are performed here. As shown in the picture, the position of the $^2A''$ symmetry resonance goes down to 3.34 eV with a width of 0.57 eV in our SEP model. The $^2A'$ symmetry resonance also becomes lower at 4.99 eV with a width of 0.87 eV in the SEP model. The $^2A''$ symmetry cross section in SE and SEP models shows a shoulder around 0.75 eV which indicates the shape resonance. However, the channel eigen phase changes smoothly in this region. It is noted that effective handling of polarization effects is very important to predict accurately the position and width of resonances for cyanamide. In Fig. 1, the $^2A'$ symmetry cross section at SEP level shows large difference from that at SE level, especially in the energy region larger than 2.0 eV. But for the $^2A''$ symmetry cross section, both SE and SEP models predict almost the same intensity except in the energy region of resonance, indicating the long range dipole potential is not important for $^2A''$ symmetry cross section.

B. Close-coupling scattering calculations

In the close-coupling (CC) scattering model, the elastic cross section and electronic excitation cross sections of electron collision with cyanamide are calculated with three different active spaces including (10, 6), (11, 4), and (11, 6). We check the cross sections and find that all of them predict the similar results. Then we use the cross sections based on the active space (11, 4) for the following discussion.

Not only shape resonance but also Feshbach resonance and core-excited resonance can be detected within the CC model. The resonance is defined as the temporary trapping of an electron to form a quasibound short-lived state. It is key for many electron-molecule scattering processes only at low energies. In the vicinity of a resonance, the cross section often changes sharply with energy, and the eigenphase sum changes by a factor of about π radians in the relatively narrow energy range. By analyzing the eigenphase sums calculated within the CC model in different active space, the resonance parameters (position and width) were obtained and listed in Table III along with their tentative assignments. It should be noted that the resonance position shifts to lower energy in higher active spaces owing to the inclusion of additional correlation effects.

The elastic cross section calculated in 12-state CI model and the active space (11, 4) is shown in Fig. 2. We find that there are two broad peaks around 4.25 eV and 6.04 eV in the total cross section. According to our phase analysis, the first broad maximum at 4.25 eV on the $^2A''$ symmetry is a π^* shape resonance with a width of 0.80 eV. The following broad maximum at 6.04 eV on the $^2A'$ symmetry belongs to σ^* shape

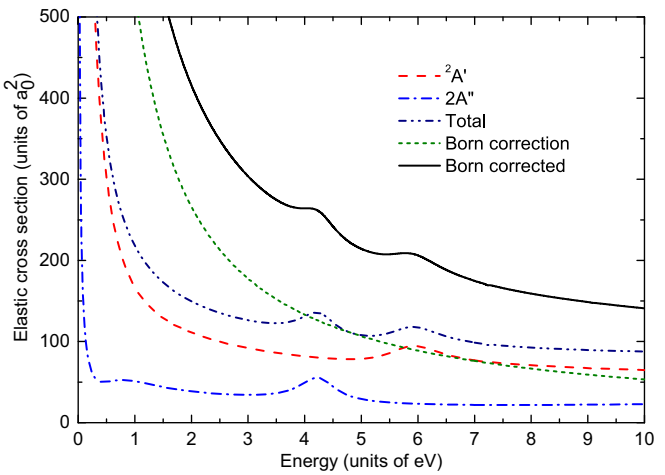

FIG. 2. Elastic cross section of the electron collision with cyanamide in the close-coupling (CC) model.

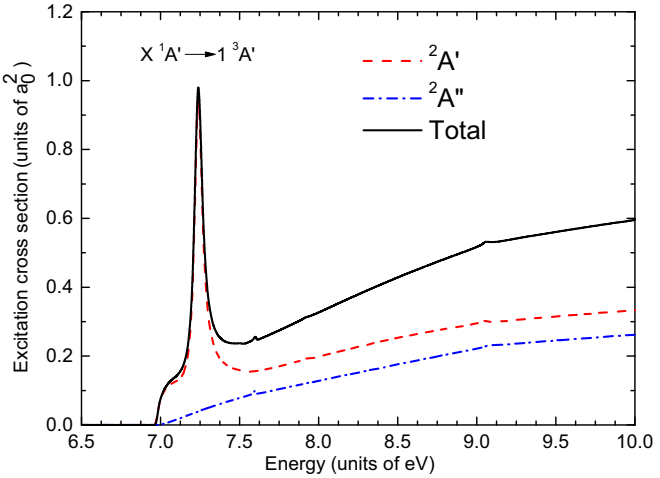

FIG. 3. Electron-impact excitation cross sections from the ground state $X\,^1A'$ to the $1\,^3A'$ state.

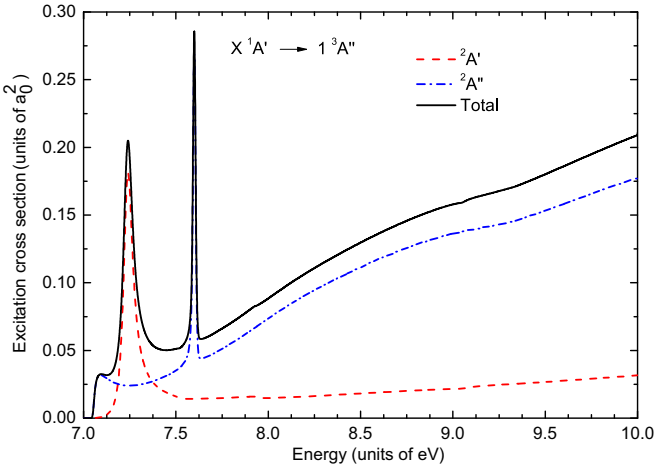

FIG. 4. Electron-impact excitation cross sections from the ground state $X\,^1A'$ to the $1\,^3A''$ state.

resonance with a width of 1.33 eV. These two shape resonances are with the ground state $X\,^1A'$ as their parent state. These two resonances are also detected in the SE calculation around 5.06 eV and 6.51 eV as mentioned in the above. Because we do not include much more virtual orbitals and double electrons excited from the active-space orbitals to virtual orbitals, the position of these two resonances in our CC model is higher than that in the SEP model.

On account of the long-range dipole interaction, the elastic cross sections are formally divergent in the fixed-nuclei approximation as the differential cross section (DCS) is singular in the forward direction. To obtain converged cross sections, the long-range scattering, dominated by interaction of higher partial waves ($l > 4$) with the molecular dipole potential, are taken into account by using a Born correction via a closure approach [19]. As shown in Fig. 2, the contribution of Born correction is larger than that of summed elastic integral cross sections in the low energies region 0–4.0 eV. This is due to that cyanamide has a large static dipole moment and the Born correction for the rotational ($0 \rightarrow 1$) component is significant.

The excitation cross sections of the transitions from the ground state $X\,^1A'$ to the first three excited states $1\,^3A'$, $1\,^3A''$, and $2\,^3A'$, are depicted in Figs. 3, 4, and 5, respectively. According to the dipole selection rules, all of them are dipole forbidden transitions. Figure 3 depicts the $X\,^1A'$ to $1\,^3A'$ excitation cross section together with the two individual contributions from $^2A'$ and $^2A''$ symmetries. The $^2A'$ contribution is slightly larger than that of the $^2A''$ symmetry. Furthermore, the total excitation cross section shows one strong sharp peak around 7.22 eV. This resonance comes from the $^2A'$ symmetry and is a Feshbach resonance whose parent state is $2\,^3A'$. The width of this resonance is 0.02 eV and the configuration is $\cdots 8a'^2 2a''^2 9a'^2 10a' 3a''$.

Figure 4 shows the $X\,^1A'$ to $1\,^3A''$ excitation cross section. As shown in the picture, the $^2A''$ contribution is much larger than that of the $^2A'$ symmetry. The strong sharp peak at 7.22 eV in $^2A'$ symmetry has been detected in the $X\,^1A' \rightarrow 1\,^3A'$ transition. The sharp peak at 7.59 eV is related to a core-excited resonance in $^2A''$ symmetry with a width of 0.02 eV and a configuration as $\cdots 8a'^2 2a''^2 9a' 10a' 3a''$. It can decay to its parent state $1\,^1A''$ if the electron of $10a'$ is detached.

In Fig. 5, we show the excited cross section to the $2\,^3A'$ state from the ground state. There are three peaks in the total cross section. The first sharp peak at 7.59 eV in $^2A''$ symmetry which we have seen in Fig. 4. The second weak peak at 7.93 eV in $^2A'$ symmetry with a width of 0.21 eV belongs to a core-excited resonance. It's parent state is $2\,^3A'$ with the configuration $\cdots 8a'^2 2a'' 9a'^2 3a'' 11a'$. The third peak at 9.06 eV is also related to a core-excited shape resonance in $^2A'$ symmetry with a width of 0.08 eV and a configuration as $\cdots 8a'^2 2a''^2 9a' 10a' 11a'$. When the electron of $10a'$ is detached, it will decay to its parent state $3\,^1A'$.

C. Dissociative electron attachment

In the present study we identify the presence of two low-lying shape resonances: one π^* resonance at 4.25 eV and the other σ^* resonance at 6.04 eV in the 12-state CI model. These shape resonances are unstable, for their large resonant width. They may decay into the ground state by detachment of the

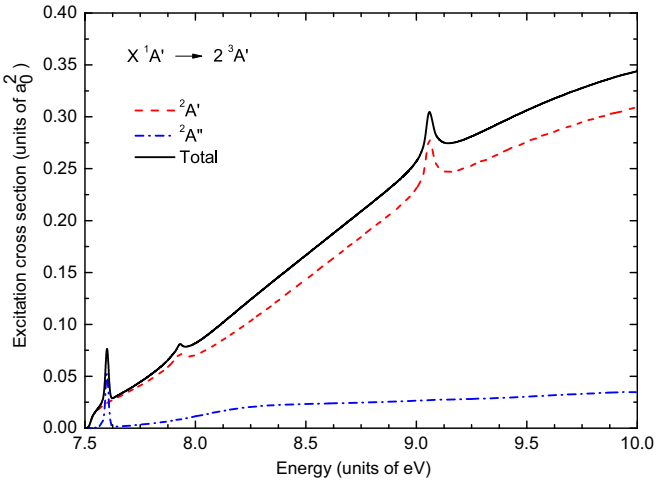

FIG. 5. Electron-impact excitation cross sections from the ground state $X\,^1A'$ to the $2\,^3A'$ state.

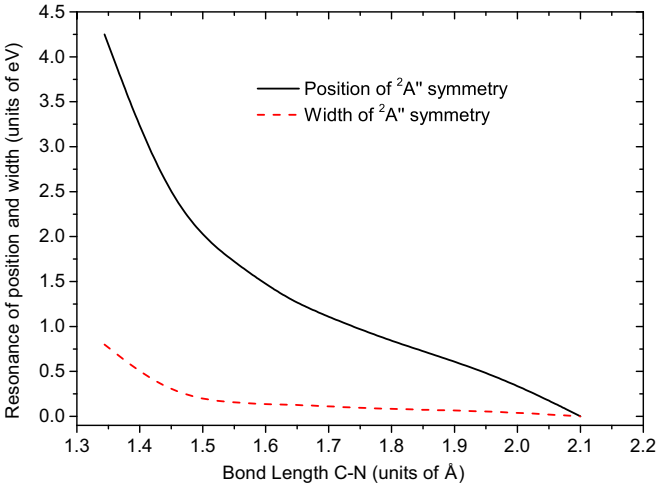

FIG. 6. Variation of π^* shape resonance width and position with stretching C-N bond length.

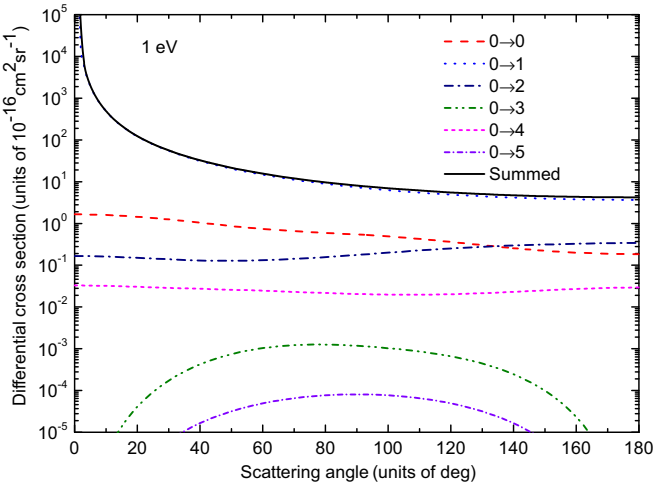

FIG. 7. Electron impact R-matrix rotationally resolved state-to-state ($J \rightarrow J'$) differential cross sections of cyanamide at 1 eV.

trapped electron. To explore the possible dissociative nature of these resonant states, we have investigated their dependence on geometry by performing a series of R-matrix calculations by stretching the C-N single bond while fixing other bond length and bond angle at equilibrium in C_s symmetry.

Figure 6 shows the position and the width of the π^* resonances change with the C-N bond stretching. When the C-N single bond is elongated, the resonance position and width decrease as expected. The width becomes to zero around 2.10 Å, which implies that this resonance become bound and support dissociative electron attachment. The electron affinity (EA) of the dissociated products also helps in assigning the preference of the scattering electron to attach to a particular fragment. Since electron affinity (EA) of CN radical (3.86 eV [15]) is much larger than that of H_2N radical (0.77 eV [15]), the most probable fragments can be CN^- ion rather than H_2C^- ion. We also performed additional calculations, not reported here for the sake of brevity, which clearly showed that neither of the shape resonances changes much its location and width when one N-H bond or both N-H bonds are stretched. Our predicted π^* resonance was regarded as precursor of the observed CN fragment in the energy region around 5.3 eV in the recent DEA experiment [6]. Our calculations show that an direct DEA pathway could take place for the C-N single bond, but the direct dissociations along the N-H bond can be ruled out. In the DEA experiment, more fragments are observed in the energy region of 6.0–9.1 eV. We also detect one σ^* shape resonance, two Feshbach resonances, and two core-excited shape resonances in the energy region of 6.0–9.5 eV. These resonances may be related with the fragments generated in DEA experiment [6]. In order to know about the dissociation dynamics via these resonances for cyanamide, one needs to explore further on the complex potential energy surfaces given by these resonant states, which is beyond the present work.

D. Differential cross section

The evaluation of differential cross section (DCS) is a stringent test for any scattering theory. In the present paper, the K-matrix based on the SEP model, the dipole moment (4.45 a.u.) and rotational constants ($A = 10.1693$ cm^{-1}, $B = 0.3302$ cm^{-1}, and $C = 0.3221$ cm^{-1}) for cyanamide are used to calculate the DCSs by using the POLYDCS program [13]. Figure 7 shows our calculated rotationally resolved DCSs for electron scattering by cyanamide at the incident energy of 1.0 eV. The elastic $0 \rightarrow 0$ component shows a minimum locates at 100°. The $0 \rightarrow 1$ contribution is much larger than the elastic $0 \rightarrow 0$ component, which results from the fact that cyanamide is a strong polar molecule. Therefore, the dominant feature of the state-resolved DCS is the dipole component $0 \rightarrow 1$. The quadrupolar component ($0 \rightarrow 2$) exhibits an almost flat behavior which is in conformity with the Born behavior. The cross section contributions of $J > 2$ are negligible, thus ensuring that our DCS has converged with respect to the J value. The DCSs obtained by summarizing the rotational cross sections for ($J = 0 \rightarrow J' = 0$–5) at the selected energies of 1, 2, 4, 6, 8, and 10 eV are depicted in Fig. 8. The large cross sections in the forward direction are due to the dipolar nature of the target. The DCSs decrease quickly with increasing

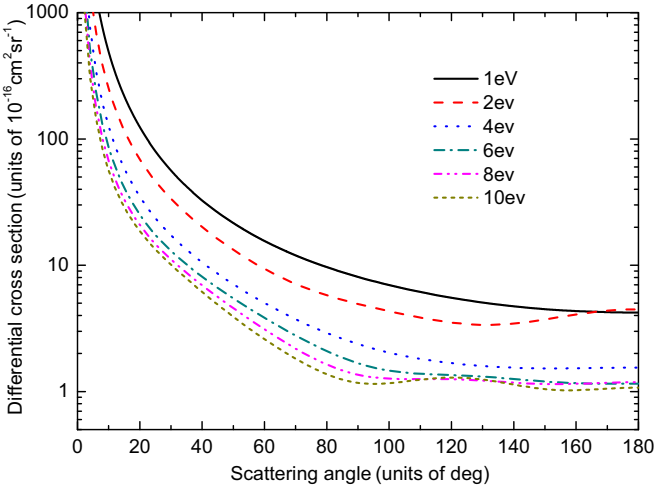

FIG. 8. Differential cross sections at 1, 2, 4, 6, 8, and 10 eV.

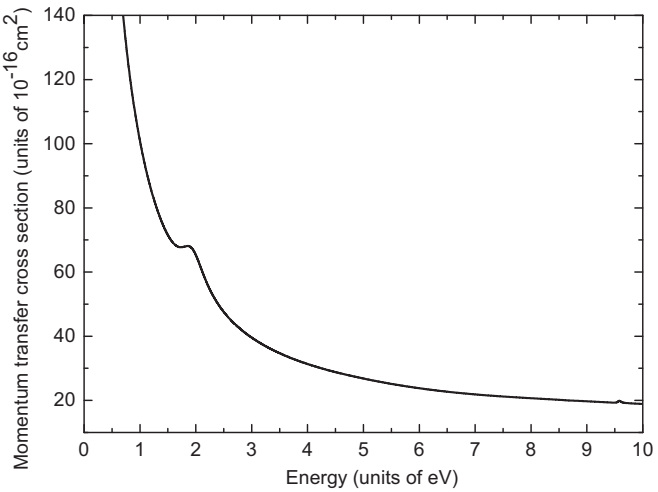

FIG. 9. Momentum transfer cross section in the energy range of 0.01–10 eV.

the scattering energy for all the scattering angles, especially for low scattering energy. To the best of our knowledge, experimental or theoretical DCS data for this molecule are still not available for comparison.

The momentum transfer cross section (MTCS) indicates the weights of backward scattering and is useful in the study of electrons drifting through a molecular gas. By using the POLYDCS program, the MTCS is calculated and presented in Fig. 9. We observe the MTCS decreases with increasing energy. In contrast to the diverging nature of DCS in the forward direction (at the small scattering angles), MTCS shows no singularity due to the multiplicative factor $(1 - \cos\theta)$, where θ is the scattering angle. It is obvious that the broad peaks of distributions for MTCS at 3.34 eV and 4.99 eV are due to the corresponding resonances.

IV. SUMMARY

We presented a detailed study of low-energy electron collisions with the cyanamide molecule. The electron-impact elastic and inelastic cross sections below 10 eV were obtained. The scattering studies were performed in three different approximations, such as SE, SEP, and CC models, with the UK molecular *R*-matrix code. We detected two shape resonance, two core-excited resonances, and two Feshbach resonances in the CC model. We check the different active spaces and find the resonance parameters are sensitive to the treatment of polarization effects. These resonances may be responsible for the various fragments observed in the DEA experiment [6]. The low-lying π^* shape resonance disappears when the C-N single bond is stretched, where it connects to a bound state, a direct DEA pathway to yield CN^- ion. The calculated DCSs show sharp increases as the scattering angle approaches zero due to the dipolar nature of the target molecule.

This detailed study involving electron collision with cyanamide should help in understanding both the basic collision behavior and the collision dynamics of the excited states of the cyanamide molecule. This work should also supplement the paucity of electron-impact collision data, which is perhaps the result of the extremely short-lived nature of these data. We hope this work will encourage others to further study the scattering phenomenon experimentally or by other *ab initio* techniques.

ACKNOWLEDGMENTS

This work was supported by the Joint Fund for Fostering Talents of National Natural Science Foundation of China and Henan Province under Grant No. U1504109, and by the National Natural Science Foundation of China under Grants No. 11604085 and No. 21303212.

[1] J. Tennyson, Phys. Rep. **491**, 29 (2010).
[2] B. Boudaffa, P. Cloutier, D. Hunting, M. A. Huels, and L. Sanche, Science **287**, 1658 (2000).
[3] J.-C. Guillemin, M. Bouyahyi, and E. H. Riague, Adv. Space Res. **33**, 81 (2004).
[4] D. Soltys, A. Rudzińska-Langwald, A. Gniazdowska, A. Wiśniewska, and R. Bogatek, Planta **236**, 1629 (2012).
[5] A. Brack, Adv. Space Res. **24**, 417 (1999).
[6] K. Tanzer, A. Pelc, S. E. Huber, Z. Czupyt, and S. Denifl, J. Chem. Phys. **142**, 034301 (2015).
[7] J. M. Carr, P. G. Galiatsatos, J. D. Gorfinkiel, A. G. Harvey, M. A. Lysaght, D. Madden, Z. Masin, M. Plummer, J. Tennyson, and H. N. Varambhia, Eur. Phys. J. D **66**, 58 (2012).
[8] K. D. Wang, Y. P. An, J. Meng, Y. F. Liu, and J. F. Sun, Phys. Rev. A **89**, 022711 (2014)
[9] K. Regeta, M. Allan, Z. Masin, and J. D. Gorfinkiel, J. Chem. Phys. **144**, 024302 (2016).
[10] S. B. Zhang, J. G. Wang, R. K. Janev, and X. J. Chen, Phys. Rev. A **82**, 062711 (2010).
[11] P. G. Burke and K. A. Berrington, *Atomic and Molecular Processes: An R-matrix Approach* (Institute of Physics, Bristol, 1993).
[12] C. J. Gillan, J. Tennyson, and P. G. Burke, in *Computational Methods for Electron-Molecule Collisions*, edited by W. M. Huo and F. A. Gianturco (Plenum, New York, 1995).
[13] N. Sana and F. A. Gianturco, Comput. Phys. Commun. **114**, 142 (1998).
[14] F. A. Gianturco and A. Jain, Phys. Rep. **143**, 347 (1986).
[15] NIST, Computational Chemistry Comparison and Benchmark Database, http://cccbdb.nist.gov.
[16] M. Birk and M. Winnewisser, Chem. Phys. Lett. **123**, 382 (1986).
[17] A. Faure, J. D. Gorfinkiel, L. A. Morgan, and J. Tennyson, Comput. Phys. Commun. **144**, 224 (2002).
[18] L. A. Morgan, C. J. Gillan, J. Tennyson, and X. Chen, J. Phys. B **30**, 4087 (1997).
[19] S. Kaur, K. L. Baluja, and J. Tennyson, Phys. Rev. A **77**, 032718 (2008).